Geophysical Journal International

On computing viscoelastic Love numbers for general planetary models: the ALMA^3 code

Journal:	*Geophysical Journal International*
Manuscript ID	GJI-21-0997
Manuscript Type:	Research Paper
Date Submitted by the Author:	02-Nov-2021
Complete List of Authors:	Melini, Daniele; Istituto Nazionale di Geofisica e Vulcanologia Spada, Giorgio; Università di Bologna, Dipartimento di Fisica e Astronomia (DIFA)
Keywords:	Tides and planetary waves < GEODESY and GRAVITY, Planetary interiors < PLANETS, Loading of the Earth < GEODESY and GRAVITY
Note: The following files were submitted by the author for peer review, but cannot be converted to PDF. You must view these files (e.g. movies) online.	
alma-sources-20211026.zip	

submitted to *Geophys. J. Int.*

On computing viscoelastic Love numbers for general planetary models: the ALMA^3 code

D. Melini[1] and G. Spada[2]

[1] *Istituto Nazionale di Geofisica e Vulcanologia (INGV), Sezione di Sismologia e Tettonofisica, Roma, Italy*

[2] *Dipartimento di Fisica e Astronomia (DIFA), Alma Mater Studiorum Università di Bologna, Italy*

SUMMARY

Love numbers for a radially stratified, viscoelastic planet are traditionally computed within the classical framework of the viscoelastic normal modes method, whose well-known shortcomings may hinder its application to models with a finely-layered structure or when complex rheological constitutive laws are assumed. Among the possible strategies to circumvent this issue, the use of a non-conventional numerical Laplace inversion scheme based upon the Post-Widder formula allows to overcome the limitations of the viscoelastic normal modes method while retaining most of its formal structure. Here we revisit the Post-Widder approach to the evaluation of loading and tidal Love numbers for an incompressible, self-gravitating, radially stratified planetary body, extending it to complex-valued Love numbers that describe the response to a periodic forcing, which are paramount in the study of the tidal deformation of planets, and to the time derivatives of Love numbers, suitable for modeling geodetic velocities in response to the variation of surface loads. We implement the numerical solution scheme in ALMA^3 (the plAnetary Love nuMbers cAlculator, version 3), an open-source Fortran 90 code that computes loading and tidal Love numbers for radially layered planetary bodies with a wide range of rheologies, including transient laws like Andrade or Burgers.

Key words: Surface loading – Tides and planetary waves – Planetary interiors.

1 INTRODUCTION

Love numbers, first introduced by A.E.H. Love in 1911, provide a complete description of the response of a planetary body to external, surface or internal perturbations. In his seminal work, Love

(1911) defined the Love numbers (LN) in the context of computing the radial deformation and the perturbation of gravity potential for an elastic, self-gravitating, homogeneous sphere that is subject to the gravitational pull of a tide-raising body. This definition has been subsequently extended by Shida (1912) to include also horizontal displacements. In order to describe the response to surface loads, an additional set of LNs, dubbed *loading Love numbers*, has been introduced in order to describe the Earth's response to surface loads (see *e.g.,* Munk & MacDonald 1960; Farrell 1972) and today they are routinely used in the context of the Post Glacial Rebound problem (Spada et al. 2011). In a similar way, *shear Love numbers* represent the response to a shear stress acting on the surface (Saito 1978) while *dislocation Love numbers* describe deformations induced by internal point dislocations (see *e.g.*, Sun & Okubo 1993).

The LN formalism has been originally defined in the realm of purely elastic deformations, for spherically symmetric Earth models consistent with global seismological observations. However, invoking the Correspondence Principle in linear viscoelasticity (see *e.g.,* Christensen 1982), the LNs can be generalized to anelastic models in a straightforward way. Currently, viscoelastic LNs are a key ingredient of several geophysical applications involving the time-dependent response of the Earth to surface loads or endogenous perturbations. For example, they are essential to the solution of the Sea Level Equation (Farrell & Clark 1976) and are exploited in current numerical implementations of the Glacial Isostatic Adjustment (GIA) problem, either on millennial (see *e.g.*, Spada & Melini 2019) or on decadal time scale (see *e.g.*, Melini et al. 2015a).

Since LNs depend on the internal structure of a planet and on its constitution, they can provide a means of establishing constraints on some physical parameters of the planet interior on the basis of geodetic measurements or astronomic observations (see *e.g.*, Zhang 1992; Kellermann et al. 2018). For tidal periodic perturbations, complex LNs can be defined in the frequency domain, accounting for both the amplitude and phase lag of the response to a given tidal frequency (Williams & Boggs 2015). Frequency-domain LNs are widely used to constrain the interior structure of planetary bodies on the basis of observations of tidal dissipation (see *e.g.,* Sohl et al. 2003; Dumoulin et al. 2017; Tobie et al. 2019), to study the state of stress of satellites induced by tidal forces (see *e.g.,* Wahr et al. 2009) or to investigate the response of giant planets (see *e.g.,* Gavrilov & Zharkov 1977).

Viscoelastic LNs for a spherically symmetric, radially layered, self-gravitating planet are traditionally computed within the framework of the "viscoelastic normal modes" method (Peltier 1974), which relies upon the solution of Laplace-transformed equilibrium equations using the formalism of elastic propagators. As discussed *e.g.* by Spada & Boschi (2006) and Melini et al. (2008), this approach becomes progressively less feasible as the detail of the rheological model is increased or if complex constitutive laws are considered. Several workarounds have been proposed in the literature

to avoid these shortcomings (see, *e.g.* Rundle 1982; Friederich & Dalkolmo 1995; Riva & Vermeersen 2002; Tanaka et al. 2006). Among these, the Post-Widder Laplace inversion formula (Post 1930; Widder 1934), first applied by Spada & Boschi (2006) to the evaluation of viscoelastic LNs for the Earth, has the advantage of maintaining unaltered the formal structure of the viscoelastic normal modes and allows a straightforward implementation of complex rheological laws.

In this work, we revisit the Post-Widder approach to the evaluation of LNs with the aim of extending it to more general planetary models, relaxing most of the assumptions originally made by Spada & Boschi (2006). In addition, we obtain Post-Widder approximations for the time derivatives of LNs, needed to model geodetic velocities in response to the variation of surface loads, and for frequency-domain LNs describing the response to periodic forcings, suitable for studying tidal dissipation in the Earth and planets. In this respect, our approach is complementary to that of Padovan et al. (2018), who derived a semi-analytical solution for the fluid LNs using the propagator formalism. We implement our results in `ALMA`^{3} (the plAnetary Love nuMbers cAlculator, version 3), an open-source code which extends and generalizes the program originally released by Spada (2008).

This paper is organized as follows. In Section 2 we give a brief outline of the theory underlying the computation of viscoelastic LNs and of the application of the Post-Widder Laplace inversion formula. In Section 3 we discuss some general aspects of `ALMA`^{3}, leaving the technical details to a User Manual. In Section 4 we benchmark numerical results with analytical solutions available for a simple model. In Section 5 we discuss some numerical examples before drawing our conclusions in Section 6.

2 MATHEMATICAL BACKGROUND

The details of the Post-Widder approach to numerical Laplace inversion have been extensively discussed in previous works (see Spada & Boschi 2006; Spada 2008; Melini et al. 2008). Here we give a brief account of the most important equations and their underlying concepts, for the sake of illustrating how it can be extended to generalized planetary models and to the case of tidal dissipation.

2.1 Viscoelastic normal modes

Closed-form analytical expressions for the LNs exist only for a few extremely simplified planetary models. The first is the homogeneous, self-gravitating sphere, often referred to as the "Kelvin sphere" (Thomson 1863). Another remarkable case is the two-layer, incompressible, non self-gravitating model that has been solved analytically by Wu & Ni (1996). For more complex models, LNs shall be computed either through fully numerical integration of the equilibrium equations, or by invoking semi-analytical schemes. Among the latter, the viscoelastic normal modes method, introduced by Peltier (1974), relies upon the solution of the equilibrium equations in the Laplace-transformed domain. In-

voking the Corrispondence Principle, the equilibrium equations can be cast in a formally elastic form by defining a complex rigidity $\mu(s)$ that depends on the rheology adopted and is a function of the Laplace variable s.

Following Spada & Boschi (2006), at a given harmonic degree n, the Laplace-transformed equations can be solved with standard propagator methods, and their solution at the planet surface ($r = a$) can be written in vector form as

$$\tilde{\mathbf{x}}(s) = \tilde{f}(s)\Big(P_1\Lambda(s)J\Big)\Big(P_2\Lambda(s)J\Big)^{-1}\mathbf{b}\,, \tag{1}$$

where the tilde denotes Laplace-transformed quantities, vector $\tilde{\mathbf{x}}(s) = (\tilde{u}, \tilde{v}, \tilde{\varphi})^T$ contains the n-th degree harmonic coefficients of the vertical ($\tilde{u}$) and horizontal ($\tilde{v}$) components of the displacement field and the incremental potential ($\tilde{\varphi}$), $\tilde{f}(s)$ is the Laplace-transformed time-history of the forcing term, P_1 and P_2 are appropriate 3×6 projection operators, J is a 6×3 array that accounts for the boundary conditions at the core interface, and $\mathbf{b}$ is a three-component vector expressing the surface boundary conditions (either of loading or of tidal type). In Eq. (1), $\Lambda(s)$ is a 6×6 array that propagates the solution from the core radius ($r = c$) to the planet surface ($r = a$), which has the form:

$$\Lambda(s) = \prod_{k=N}^{1} Y_k(r_{k+1}, s)Y_k^{-1}(r_k, s)\,, \tag{2}$$

where N is the number of homogeneous layers outside the planet core, r_k is the radius of the interface between the $(k-1)$-th and k-th layer, with $r_1 \leq ... \leq r_N$, $r_1 = c$ and $r_{N+1} = a$. In Eq. (2), $Y_k(r, s)$ is the fundamental matrix that contains the six linearly independent solutions of the equilibrium equations valid in the k-th layer, whose expressions are given analytically in Sabadini et al. (1982). When incompressibility is assumed, the matrix $Y_k(r, s)$ depends upon the rheological constitutive law through the functional form of the complex rigidity $\mu(s)$, which replaces the elastic rigidity μ of the elastic propagator (Wu & Peltier 1982). Table 1 lists expressions of $\mu(s)$ for some rheological laws. For a fluid inviscid (*i.e.,* zero viscosity) core, the array J in Eq. (1) is a 6×3 interface matrix whose components are explicitly given by Sabadini et al. (1982); otherwise J corresponds to the 6×3 portion of the fundamental matrix for the core $Y_c(c, s)$ that contains the three solutions behaving regularly for $r \mapsto 0$.

From the solution $\tilde{\mathbf{x}}(s)$ obtained in (1), the Laplace-transformed Love Numbers are defined as:

$$\tilde{h}_n(s) = \frac{m}{a}\tilde{u}_n(s) \tag{3}$$

$$\tilde{l}_n(s) = \frac{m}{a}\tilde{v}_n(s) \tag{4}$$

$$\tilde{k}_n(s) = -1 - \frac{m}{ag}\tilde{\varphi}_n(s)\,, \tag{5}$$

where we have made the n-dependence explicit, m is the planet mass and g is the unperturbed surface gravitational acceleration (Farrell 1972; Wu & Peltier 1982). Using Cauchy's residue theorem, for

Maxwell or generalized Maxwell rheologies Eqs. (3-5) can be cast in the standard normal modes form, which for an impulsive load ($\tilde{f}(s) = 1$) reads

$$\tilde{L}_n(s) = L_n^e + \sum_{k=1}^{N_M} \frac{L_n^k}{s - s_n^k}\,, \tag{6}$$

where $\tilde{L}_n(s)$ denotes any of the three LNs, L_n^e is the elastic component of the LN (*i.e.,* the limit for $s \mapsto \infty$), L_n^k are the viscoelastic components (residues), s_n^k are the (real and negative) roots of the secular equation $\mathrm{Det}(P_2 \Lambda(s) J) = 0$, and where N_M is the number of viscoelastic normal modes, each corresponding to one root of the secular equation (Spada & Boschi 2006). However, such standard form is not always available, since for some particular rheologies the complex rigidity $\mu(s)$ cannot be cast in the form of a rational fraction (this occurs, for example, for the Andrade's rheology, see Table 1). This is one of the motivations for adopting non-conventional Laplace inversion formulas like the one discussed in next section.

2.2 Love numbers in the time domain

To obtain the time-domain LNs $h_n(t)$, $l_n(t)$ and $k_n(t)$, it is necessary to perform the inverse Laplace transform of Eqs. (3-5). Within the viscoelastic normal mode approach, this is usually accomplished through an integration over a (modified) Bromwich path in the complex plane, by invoking the residue theorem. In this case, the inversion of Eq. (6) yields the time-domain Love numbers in the form:

$$L_n(t) = L_n^e \delta(t) + H(t) \sum_{k=1}^{M} L_n^k \mathrm{e}^{s_n^k t}\,, \tag{7}$$

where $\delta(t)$ is the Dirac delta and $H(t)$ is the Heaviside step function defined by Eq. (14) below, and an impulsive time history is assumed ($\tilde{f}(s) = 1$). As discussed by Spada & Boschi (2006), the traditional scheme of the viscoelastic normal modes suffers from a few but significant shortcomings that, with models of increasing complexity, effectively hinders a reliable numerical inverse transformation. Indeed, the application of the residue theorem demands the identification of the poles of the Laplace-transformed solutions (see Eqs. 3-5), which are the roots of a polynomial equation whose degree increases with the number of rheologically distinct layers. In addition, its algebraic complexity may be difficult to handle, particularly for constitutive laws characterized by many material parameters.

As shown by Spada & Boschi (2006) and Spada (2008), a possible way to circumvent these difficulties is to compute the inverse Laplace transform through the Post-Widder (PW) formula (Post 1930; Widder 1934). We note, however, that other viable possibilities exist, as the one recently discussed by Michel & Boy (2021), who have employed Fourier techniques to avoid some of the problems inherent in the Laplace transform method. If $\tilde{F}(s) = \mathcal{L}(F(t))$ is the Laplace transform of $F(t)$, the PW for-

mula gives an asymptotic approximation of the inverse Laplace transform $\mathcal{L}^{-1}(\tilde{F}(s))$ as a function of the n-th derivatives of $\tilde{F}(s)$ evaluated along the real positive axis:

$$F(t) = \lim_{n\to\infty} \frac{(-1)^n}{n!} \left(\frac{n}{t}\right)^{n+1} \left[\frac{d^n}{ds^n}\tilde{F}(s)\right]_{s=\frac{n}{t}} . \tag{8}$$

In general, an analytical expression for the n-th derivative of $\tilde{F}(s)$ required in Eq. (8) is not available. By employing a recursive discrete approximation of the derivative and rearranging the corresponding terms, Gaver (1966) has shown that an equivalent expression is

$$F(t) = \lim_{n\to\infty} \frac{n\ln 2}{t} \binom{2n}{n} \sum_{j=0}^{n} (-1)^j \binom{n}{j} \tilde{F}\left(\frac{(n+j)\ln 2}{t}\right) , \tag{9}$$

where the inverse transform $F(t)$ is expressed in terms of samples of the Laplace transform $\tilde{F}(s)$ on the real positive axis of the complex plane. Since for a stably stratified incompressible planet all the singularities of $\tilde{\mathbf{x}}(s)$ (Eq. 1) are expected to be located along the real negative axis that ensures the long-term gravitational stability (Vermeersen & Mitrovica 2000), Eq. (9) provides a strategy for evaluating the time-dependent LNs without the numerical complexities associated with the traditional contour integration. However, as discussed by Valkó & Abate (2004), the numerical convergence of (9) is logarithmically slow, and the oscillating terms can lead to catastrophic loss of numerical precision. Stehfest (1970) has shown that, for practical applications, the convergence of Eq. (9) can be accelerated by re-writing it in the form

$$F(t) = \lim_{M\to\infty} \frac{\ln 2}{t} \sum_{j=1}^{2M} \zeta_{j,M} \tilde{F}\left(\frac{j\ln 2}{t}\right) , \tag{10}$$

where M is the order of the Gaver sequence and where the ζ constants are defined as

$$\zeta_{k,M} = (-1)^{M+k} \sum_{j=\mathrm{floor}\left(\frac{k+1}{2}\right)}^{\min(M,k)} \frac{j^{M+1}}{M!} \binom{M}{j} \binom{2j}{j} \binom{j}{k-j} , \tag{11}$$

with $\mathrm{floor}(x)$ being the greatest integer less or equal to x. Eq. (10) can be applied to (1) to obtain an M-th order approximation of the time-domain solution vector:

$$\mathbf{x}^{(M)}(t) = \frac{\ln 2}{t} \sum_{j=1}^{2M} \zeta_{j,M}\, \tilde{\mathbf{x}}\left(\frac{j\ln 2}{t}\right) , \tag{12}$$

from which the time-domain LNs can be readily obtained according to Eqs. (3-5).

Recalling that the Laplace transform of $F(t)$ and that of its time derivative $\dot{F}(t)$ are related by $\mathcal{L}(\dot{F}(t)) = s\mathcal{L}(F(t)) - F(0^-)$ and being $\mathbf{x}(t) = 0$ for $t < 0$, it is also possible to write an asymptotic approximation for the time derivative of the solution:

$$\dot{\mathbf{x}}^{(M)}(t) = \left(\frac{\ln 2}{t}\right)^2 \sum_{j=1}^{2M} j\, \zeta_{j,M}\, \tilde{\mathbf{x}}\left(\frac{j\ln 2}{t}\right) , \tag{13}$$

from which the time derivative of the LNs $\dot{h}_n(t)$, $\dot{l}_n(t)$ and $\dot{k}_n(t)$ can be obtained according to Eqs. (3-5).

The time dependence of the solution vector obtained through Eqs. (12-13) is also determined by the time history of the forcing term (either of loading or tidal type), whose Laplace transform $\tilde{f}(s)$ appears in Eq. (1). If the loading is instantaneously switched on at $t = 0$, its time history is represented by the Heaviside step function

$$H(t) = \begin{cases} 0, & t \leq 0 \\ 1, & t > 0\,, \end{cases} \tag{14}$$

whose Laplace transform is

$$\tilde{H}(s) = \mathcal{L}(H(t)) = \frac{1}{s}\,. \tag{15}$$

Since any piece-wise constant function can be expressed as a linear combination of shifted Heaviside step functions (see, *e.g.* Spada & Melini 2019), LNs obtained assuming the loading time history in Eq. (14) can be used to compute the response to arbitrary piece-wise constant loads. However, for some applications, it may be more convenient to represent the load time history as a piece-wise linear function. It is easy to show that any such function can be written as a linear combination of shifted *elementary ramp functions* of length t_r, of the type

$$R(t) = \begin{cases} 0, & t \leq 0 \\ \dfrac{t}{t_r}, & 0 < t \leq t_r \\ 1, & t > t_r\,, \end{cases} \tag{16}$$

whose Laplace transform is

$$\tilde{R}(s) = \mathcal{L}(R(t)) = \frac{1}{s} \cdot \frac{1 - e^{-s t_r}}{s\, t_r}\,. \tag{17}$$

Laplace-transformed LNs corresponding to a step-wise or ramp-wise forcing time history can be obtained by setting $\tilde{f}(s) = \tilde{H}(s)$ or $\tilde{f}(s) = \tilde{R}(s)$ in Eq. (1), respectively.

2.3 Love numbers in the frequency domain

In the context of planetary tidal deformation, it is important to determine the response to an external periodic tidal potential. In that case, the time dependence of the forcing term has the harmonic form $e^{i\omega t}$, where $\omega = 2\pi/T$ is the angular frequency of the forcing term, T is its period and $i = \sqrt{-1}$ is the imaginary unit. In the time domain, the solution vector can be expressed as

$$\mathbf{x}_\omega(t) = \mathbf{x}_\delta(t) * e^{i\omega t}\,, \tag{18}$$

where $\mathbf{x}_\delta(t)$ is the time-domain response to an impulsive (δ-like) load and the symbol $*$ indicates

the time convolution. Since the impulsive load is causal, $\mathbf{x}_\delta(t) = 0$ for $t < 0$ and Eq. (18) can be equivalently written as

$$\mathbf{x}_\omega(t) = e^{i\omega t} \int_0^\infty \mathbf{x}_\delta(t') e^{-i\omega t'} dt' = \mathbf{x}_0(\omega) e^{i\omega t} \,, \tag{19}$$

where $\mathbf{x}_0(\omega)$ is the Laplace transform of $\mathbf{x}_\delta(t)$ evaluated at $s = i\omega$. By setting $\tilde{f}(s) = \mathcal{L}(\delta(t)) = 1$ and $s = i\omega$ in Eq. (1), we obtain

$$\mathbf{x}_0(\omega) = \Big(P_1 \Lambda(i\omega) J\Big) \Big(P_2 \Lambda(i\omega) J\Big)^{-1} \mathbf{b} \,. \tag{20}$$

In analogy with Eqs. (3-5), the frequency-domain LNs $h_n(\omega)$, $l_n(\omega)$ and $k_n(\omega)$ are defined as

$$h_n(\omega) = \frac{m}{a} u_n(\omega) \tag{21}$$

$$l_n(\omega) = \frac{m}{a} v_n(\omega) \tag{22}$$

$$k_n(\omega) = -1 - \frac{m}{ag} \varphi_n(\omega) \,, \tag{23}$$

where $u_n(\omega)$, $v_n(\omega)$ and $\varphi_n(\omega)$ are the three components of vector $\mathbf{x}_0(\omega) = (u_n, v_n, \varphi_n)^T$.

Since the frequency-domain LNs are complex numbers, in general there is a phase difference between the variation of the external periodic potential and the planet response, due to the energy dissipation within the planetary mantle. If $L_n(\omega)$ is any of the three frequency-domain LNs, we have

$$L_n(t) = L_n(\omega) e^{i\omega t} = |L_n(\omega)| e^{i(\omega t - \phi)} \,, \tag{24}$$

where the *phase lag* ϕ is given by

$$\tan\phi = -\frac{\mathrm{Im}(L_n(\omega))}{\mathrm{Re}(L_n(\omega))} \,, \tag{25}$$

and $\mathrm{Re}(z)$ and $\mathrm{Im}(z)$ denote the real and the imaginary parts of z, respectively. A vanishing phase lag ($\phi = 0$) is only expected for elastic planetary models (*i.e.,* for $\mathrm{Im}(L_n(\omega)) = 0$).

Tidal dissipation is customarily expressed in term of the *quality factor* Q (Kaula 1964; Goldreich & Soter 1966), which according to *e.g.* Efroimsky & Lainey (2007) and Clausen & Tilgner (2015) is related to the phase lag ϕ through

$$Q(\omega) = \frac{1}{\sin\phi} = -\frac{|L_2(\omega)|}{\mathrm{Im}\,(L_2(\omega))} \,, \tag{26}$$

thus implying $Q = \infty$ in the case of no dissipation. For terrestrial bodies, the quality factor Q usually lies in a range between 10 and 500 (Goldreich & Soter 1966; Murray & Dermott 2000). We note that in experimental applications, tidal dissipation is often measured through the ratio

$$\frac{k_2}{Q} = k_2 \sin\phi \,, \tag{27}$$

which for $|\mathrm{Im}\, k_2| \ll |k_2|$ can be approximated as

$$\frac{k_2}{Q} \simeq -\mathrm{Im}\, k_2 \,. \tag{28}$$

3 AN OVERVIEW OF ALMA^3

In this section we briefly outline how the solution scheme described in the previous Section has been implemented in program ALMA^3, leaving the technical details and practical considerations to the accompanying User Manual. ALMA^3 can evaluate, for any given harmonic degree n, the time-domain LNs $(h_n(t), l_n(t), k_n(t))$, their time derivatives $(\dot{h}_n(t), \dot{l}_n(t), \dot{k}_n(t))$ and the frequency-domain LNs $(h_n(\omega), l_n(\omega), k_n(\omega))$, either corresponding to surface loading or to tidal boundary conditions. The planetary model can include, in principle, any number of layers in addition to a central core. Each of the layers can be characterized by any of the rheological laws listed in Table 1, while the core can also have a fluid inviscid rheology.

Time-domain LNs are computed by evaluating numerically Eqs. (12) and (13), assuming a time history of the forcing that can be either a step function (Eq. 14) or an elementary ramp (Eq. 16). In the latter case, the duration t_r of the loading phase can be configured by the user. Since Eqs. (12) and (13) are singular for $t = 0$, ALMA^3 can compute time-domain LNs only for $t > 0$. In the "elastic limit", the LNs can be obtained by configuring the Hooke's elastic rheology for all the layers in the model; of course, in this case, the LNs will follow the same time history of the forcing. As discussed in Section 2, the sums in Eqs. (12) and (13) contain oscillating terms that can lead to loss of precision due to catastrophic cancellation (Spada & Boschi 2006). To avoid the consequent numerical degeneration of the LNs, ALMA^3 performs all computations in arbitrary-precision floating point arithmetic, using the Fortran FMLIB library (Smith 1991, 2003).

When running ALMA^3, the user shall configure both the number D of significant digits used by the FMLIB library and the order M of the Gaver sequence in Eqs. (12) and (13). Higher values of D and M ensure a better numerical stability and accuracy of the results, but come at the cost of rapidly increasing computation time. All the examples discussed in the next Section have been obtained with $D = 128$, $M = 8$. While these values ensure a good stability in relatively simple models, a special care shall be devoted to numerical convergence in case of models with a large number of layers and/or when computing LNs to high harmonic degrees; in that case, higher values of D and M may be needed to attain stable results.

Frequency-domain LNs are obtained by ALMA^3 by directly sampling Eq. (20) at the requested frequencies ω. While the evaluation of frequency-domain LNs is less prone to numerical degeneration, a high numerical precision may still be needed, especially in case of models including a large number of layers. ALMA^3 does not directly compute the tidal phase lag ϕ, the quality factor Q nor the k_2/Q ratio, which can be readily obtained from tabulated output values of the real and imaginary parts of LNs through Eqs. (25-27).

4 BENCHMARKING ALMA^3 WITH THE VISCOELASTIC KELVIN SPHERE

Simplified planetary models for which closed-form expressions for the LNs are available are of particular relevance here, since they allow an analytical benchmarking of the numerical solutions discussed in Section 2 and provided by ALMA^3.

In what follows, we consider a spherical, homogeneous, self-gravitating model, often referred to as the "Kelvin sphere" (Thomson 1863), which can be extended to a viscoelastic rheology in a straightforward manner. For example, adopting the the complex modulus $\mu(s)$ appropriate for the Maxwell rheology (see Table 1), for a Kelvin sphere of radius a, density ρ and surface gravity g, in the Laplace domain the harmonic degree $n = 2$ LNs take the form

$$\tilde{L}_2(s) = \frac{L_f}{1 + \gamma^2 \dfrac{s}{s + 1/\tau}}\,, \tag{29}$$

where L_2 is any of (h_2, l_2, k_2), L_f is the "fluid limit" of $\tilde{L}_2(s)$ (*i.e.,* the value attained for $s \to 0$), $\tau = \eta/\mu$ is the Maxwell relaxation time and

$$\gamma^2 = \frac{19}{2}\frac{\mu}{\rho g a} \tag{30}$$

is a positive non-dimensional constant. Note that g is a function of a and ρ, since for the homogeneous sphere $g = \frac{4}{3}\pi G \rho a$, where G is the gravitational constant.

After some algebra, (29) can be cast in the form

$$\tilde{L}_2(s) = \frac{L_f}{1 + \gamma^2}\left(1 + \frac{1/\tau - 1/\tau'}{s + 1/\tau'}\right)\,, \tag{31}$$

where for a tidal forcing, the fluid limits for $n = 2$ are $h_f = \frac{5}{2}$, $l_f = \frac{3}{4}$ and $k_f = \frac{3}{2}$ (see *e.g.*, Lambeck 1988) and where we have defined the new time scale $\tau' = (1 + \gamma^2)\tau$. From Eq. (31), the LNs in the time domain can be immediately computed analytically through an inverse transformation:

$$L_2(t) = \frac{L_f}{1 + \gamma^2}\left[\delta(t) + H(t)\left(\frac{1}{\tau} - \frac{1}{\tau'}\right)e^{-t/\tau'}\right]\,, \tag{32}$$

while for an external forcing characterized by a step-wise time-history, the LNs $L_2^{(H)}(t)$ are obtained by a convolution of Eq. (32) with the Heaviside function:

$$L_2^{(H)}(t) = L_2(t) * H(t)\,, \tag{33}$$

which yields

$$L_2^{(H)}(t) = \frac{L_f}{1 + \gamma^2}\left[1 + \gamma^2\left(1 - e^{-t/\tau'}\right)\right]\,, \quad t \geq 0\,, \tag{34}$$

from which the time derivative of $L_2^{(H)}(t)$ is readily obtained:

$$\dot{L}_2^{(H)}(t) = \frac{L_f}{1 + \gamma^2}\left(\frac{1}{\tau} - \frac{1}{\tau'}\right)e^{-t/\tau'}\,, \quad t > 0\,. \tag{35}$$

F1 In Figure 1a, the dotted curves show the h_2 (blue) and the k_2 (red) tidal LN of harmonic degree

$n = 2$ obtained by a configuration of ALMA^3 that reproduces the Kelvin sphere (the parameters are given in the caption). The LNs, shown as a function of time, are characterized by two asymptotes corresponding to the elastic and fluid limits, respectively, and by a smooth transition in between. The solid curves, obtained by the analytical expression given by Eq. (34), show an excellent agreement with the ALMA^3 numerical solutions. The same holds for the time-derivatives of these LNs, considered in Figure 1b, where the analytical LNs (solid lines) are computed according to Eq. (35).

The frequency response of the Kelvin sphere for a periodic tidal potential can be obtained by setting $s = i\omega$ in Eq. (29), which after rearranging gives:

$$L_2(\omega) = \frac{L_f}{1+\gamma^2}\left[1 + \frac{\gamma^2}{1+(\omega\tau')^2} - i\gamma^2\frac{\omega\tau'}{1+(\omega\tau')^2}\right], \tag{36}$$

which remarkably depends upon ω and τ only through the $\omega\tau$ product. Therefore, a change in the relaxation time τ shall result in a shift of the frequency response of the Kelvin sphere, leaving its shape unaltered.

Using Eq. (36) in (25), the phase lag is:

$$\tan\phi = \frac{\gamma^2\omega\tau}{1+\omega^2\tau\tau'}, \tag{37}$$

where it is easy to show that for frequency

$$\omega_0 = \frac{1}{\sqrt{\tau\tau'}} \tag{38}$$

the maximum phase lag $\phi = \phi_{max}$ is attained, with

$$\tan\phi_{max} = \frac{\gamma^2}{2\sqrt{1+\gamma^2}}. \tag{39}$$

By using Eq. (36) in (26), the quality factor Q for the Kelvin sphere is

$$Q_K(\omega) = \sqrt{1 + \frac{1}{\gamma^4}\left(\omega\tau' + \frac{1}{\omega\tau}\right)^2}, \tag{40}$$

which at $\omega = \omega_0$ attains its minimum value

$$Q_{min} = 1 + \frac{2}{\gamma^2}. \tag{41}$$

In Figure 2a, the dotted curve shows the phase lag ϕ as a function of the tidal period $T = 2\pi/\omega$, obtained by the same configuration of ALMA^3 described in the caption of Figure 1. The solid line corresponds to the analytical expression of $\phi(T)$ which can be obtained from Eq. (37), showing once again an excellent agreement with the numerical results (dotted). Figure 2b compares numerical results obtained from ALMA^3 for Q with the analytical expression for $Q_K(T)$ obtained from (40). By using in Eq. (38) the numerical values of ρ, a and μ assumed in Figures 1 and 2, the period $T_0 = 2\pi/\omega_0$ is found to scale with viscosity η as

$$T_0 = (3.06\,\mathrm{kyr})\left(\frac{\eta}{10^{21}\,\mathrm{Pa\cdot s}}\right), \tag{42}$$

so that for $\eta = 10^{21}\,\mathrm{Pa}\cdot\mathrm{s}$, representative of the Earth's mantle bulk viscosity (see *e.g.,* Mitrovica 1996; Turcotte & Schubert 2014), the maximum phase lag $\phi_{max} \simeq 41.9^\circ$ and the minimum quality factor $Q_{min} \simeq 1.5$ are attained for $T_0 \simeq 3\,\mathrm{kyr}$, consistent with the results shown in Figure 2.

5 EXAMPLES

Next we consider three applications showing the potential of `ALMA`^{3} in different contexts. First we will discuss the evaluation of tidal LNs for Enceladus, in order to show how an internal fluid layer can be simulated as a low-viscosity newtonian fluid rheology. Then, we will evaluate a set of loading LNs suitable for describing the transient response of the Earth to the melting of large continental ice sheets. As a last example, we will demonstrate how `ALMA`^{3} can simulate the tidal dissipation on the Moon using two recent interior models based on seismological data.

5.1 Tidal Love numbers of Enceladus

The scientific interest on Enceladus has gained considerable momentum after the 2005 Cassini flybys, which confirmed the icy nature of its surface and evidenced the existence of water-rich plumes emerging from the southern polar regions (Porco et al. 2006; Ivins et al. 2020). These hint to the existence of a subsurface ocean, heated by tidal dissipation in the core, where physical conditions allowing life could be possible, in principle (for a review, see Hemingway et al. 2018). The interior structure of Enceladus has been thoroughly investigated in literature on the basis of observations of its gravity field (Iess et al. 2014), tidal deformation and physical librations (see, *e.g.* Čadek et al. 2016), setting constraints on the possible structure of the ice shell and of the underlying liquid ocean (Roberts & Nimmo 2008), and on the composition of its core (Roberts 2015).

While a thorough investigation of the signature of the interior structure of Enceladus on its tidal response is far beyond the scope of this work, here we briefly illustrate how the LNs for a planetary body including a fluid internal layer can be computed with `ALMA`^{3}. To this aim, we have set up a model including an homogeneous inner solid core of radius $c = 190$ km and density $\rho_c = 2400$ kg·m^{-3} (Hemingway et al. 2018), surrounded by a liquid water layer and an outer icy shell, and investigate the sensitivity of the k_2 tidal LN to the thickness of the ice layer, along the lines of Roberts & Nimmo (2008). In our setup, the core is modeled as a Maxwell body with rigidity $\mu_c = 10^{11}$ Pa and viscosity $\eta_c = 10^{17}$ Pa·s. Since in `ALMA`^{3} a fluid inviscid rheology can be prescribed only for the core, we approximate the ocean layer as a low-viscosity Newtonian fluid with viscosity $\eta_w = 10^5$ Pa·s. The ice shell is modeled as a Maxwell body with viscosity $\eta_i = 10^{13}$ Pa·s and rigidity $\mu_i = 4\times10^9$ Pa, a value consistent with evidence from tidal flexure of marine ice (Vaughan 1995) and laboratory experiments

(Cole & Durell 1995). The densities of ice and water are set to $\rho_i = 950$ kg·m^{-3} and $\rho_w = 1000$ kg·m^{-3}, respectively.

In Figure 3, the blue curves show the modulus of the k_2 tidal LN (frame a), its phase lag ϕ (b) and the quality factor $Q = 1/\sin\phi$ (c) as a function of the thickness of the ice layer, for a forcing period $T = 1.37$ days. This period corresponds to the shortest librational oscillation of Enceladus (Rambaux et al. 2010). A marked sensitivity of $|k_2|$ to the thickness of the ice shell is apparent, with values decreasing from ~ 0.6 for a very thin shell to less than ~ 0.05 if no ocean is present. Frames (b) and (c) show that the tidal dissipation increases strongly with the thickness of the ice shell. To investigate the effect of the viscosity structure of the ice on the tidal response, we have modified our model by introducing an high-viscosity icy lithosphere ($\eta_l = 10^{19}$ Pa·s) in the outer half of the ice layer. Numerical results for this second model are shown by red curves in Figure 3. While $|k_2|$ still has a strong sensitivity to the thickness of the ice layer even in presence of a lithosphere (a), tidal dissipation (b and c) is strongly attenuated in presence of the lithosphere. These results suggest that the viscosity structure of the ice shell may be a major factor controlling tidal dissipation on Enceladus. F3

5.2 Loading Love numbers for transient rheologies

Loading Love numbers are key components in models of the response of the Earth to the spatio-temporal variation of surface loads, including the ongoing deformation due to the melting of the late Pleistocene ice complexes (see *e.g.,* Peltier & Drummond 2008; Purcell et al. 2016), the present-day and future response to climate-driven melting of ice sheets and glaciers (Bamber & Riva 2010; Slangen 2012), and deformations induced by the variation of hydrological loads (Bevis et al. 2016; Silverii et al. 2016). Evidence from Global Navigation Satellite System measurements of the time-dependent surface deformation point to a possible transient nature of the mantle in response to the regional-scale melting of ice sheets and to large earthquakes (see, *e.g.*, Pollitz 2003, 2005; Nield et al. 2014; Qiu et al. 2018). Here, it is therefore of interest to present the outcomes of some numerical experiments in which `ALMA`[3] is configured to compute the time-dependent h loading Love Number assuming a transient rheology in the mantle. Numerical estimates of $h_n(t)$ and of its time derivative $\dot{h}_n(t)$ would be needed, for instance, to model the response to the thickness variation of a disc-shaped surface load, as discussed by Bevis et al. (2016).

In Figure 4 we show the time evolution of the $h_n(t)$ loading LN for $n = 2, 10$ and 100, comparing the response obtained assuming the VM5a viscosity model of Peltier & Drummond (2008), which is fully based on a Maxwell rheology, with those expected if VM5a is modified introducing a transient rheology in the upper mantle layers. An Heaviside time history for the load is adopted throughout. In model VM5a-BG we assumed a Burgers bi-viscous rheological law in the upper mantle, with $\mu_2 = \mu_1$ F4

and $\eta_2/\eta_1 = 0.1$ (see Table 1), while in model VM5a-AD an Andrade rheology (Cottrell 1996) with creep parameter $\alpha = 0.3$ has been assumed for the upper mantle. For $n = 2$ (Figure 4a) the responses obtained with the three models almost overlap. Indeed, for long wavelengths (by Jean's rule, the wavelength corresponding to harmonic degree n is $\lambda = \frac{2\pi a}{n+\frac{1}{2}}$) the response to surface loads is mostly sensitive to the structure of the lower mantle, where the three variants of VM5a considered here have the same rheological properties. Conversely, for $n = 10$ (b) we see a slightly faster response to the loading for both transient models in the time range between 0.01 and 1 kyr. For $n = 100$, the transient response of VM5a-BG and VM5a-AD becomes even more enhanced between 0.01 and 10 kyr. It is worth to note that, for times less than ~ 10 kyr, the two transient versions of VM5a almost yield identical responses, suggesting that an Andrade rheology in the Earth's upper mantle might explain the observed vertical transient deformations in the same way as a Burgers rheology. The differences between the three models are more evident in Figure 5, where the time derivatives $\dot{h}_n(t)$ are shown. Compared with the Maxwell model, the transient ones show a significantly larger initial rate of vertical displacement, that differ significantly for Burgers and Andrade. The three rheologies provide the same response only ~ 0.1 kyrs after loading.

5.3 Tidal dissipation on the Moon

The Moon is the extraterrestrial body for which the most detailed information about the internal structure is available. In addition to physical constraints from observations of tidal deformation (Williams et al. 2014), seismic experiments deployed during the Apollo missions (Nunn et al. 2020) provided instrumental recordings of moonquakes which allowed the formulation of a set of progressively refined interior models (see, *e.g.* Heffels et al. 2021).

In this last numerical experiment, we configured `ALMA`^{3} to compute tidal LNs for the Moon corresponding to the two interior models proposed by Weber et al. (2011, W11 hereafter) and Garcia et al. (2011, 2012, G12 hereafter). Profiles of density ρ and rigidity μ for models W11 and G12 are shown in Figure 6, with the most notable difference being that the former assumes an inner solid core and a fluid outer core, while the latter contains an undifferentiated fluid core. For both models, we assumed a Maxwell rheology in the crust and the mantle, with a viscosity of 10^{20} Pa·s. The fluid core has been modeled as a Newtonian fluid with viscosity 10^4 Pa·s while in the inner core, for model W11, we used a Maxwell rheology with a viscosity of 10^{16} Pa·s, a value within the estimated ranges for the viscosity of the Earth inner core (Buffett 1997; Dumberry & Mound 2010; Koot & Dumberry 2011). Following the lines of Harada et al. (2014, 2016) and Organowski & Dumberry (2020), we defined a 150 km thick low-viscosity zone (LVZ) at the base of the mantle and computed the k_2 tidal LNs as a function of the LVZ viscosity for a forcing period $T = 27.212$ days.

For both W11 and G12 models, Figure 7 shows the dependence on the LVZ viscosity of the k_2 tidal LN (frame a), of its phase lag angle (b) and of the quality factor Q (c). With the considered setup, for a LVZ viscosity smaller than 10^{15} Pa·s the tidal response of the two models is almost coincident, while for higher viscosities model G12 predicts a stronger tidal dissipation. Shaded gray areas in frames (a) and (c) show 1-σ confidence intervals for experimental estimates of k_2 (Williams et al. 2014) and Q (Williams & Boggs 2015). With both models we obtain values of k_2 within the 1-σ interval for an LVZ viscosity smaller than about 5×10^{15} Pa·s; interestingly, for that LVZ viscosity the G12 model predicts a quality factor Q within the measured range, while model W11 would require a slightly higher LVZ viscosity (10^{16} Pa·s). Of course, a detailed assessment of the ability of the two models to reproduce the observed tidal LNs would be well beyond the scope of this work, and several additional parameters potentially affecting the tidal response (as *e.g.* the LVZ thickness or the core radius) would need to be considered. F7

6 CONCLUSIONS

We have discussed how the Post-Widder approach to the evaluation of viscolestic Love numbers can be generalized for arbitrary planetary models and extended to the case of complex-valued LNs suitable for studying tidal dissipation. Our results are the basis of `ALMA`^{3}, a user friendly Fortran program that computes the Love numbers of a multi-layered, self-gravitating, spherically symmetric, incompressible planetary model characterized by a linear viscoelastic rheology. `ALMA`^{3} can be suitably employed to solve a wide range of problems, either involving the surface loading or the tidal response of a rheologically layered planet. By taking advantage of the Post-Widder Laplace inversion method, the evaluation of the time-domain Love numbers is simplified, avoiding some of the limitations of the traditional viscoelastic normal mode approach. Differently from previous implementations (Spada 2008), `ALMA`^{3} can evaluate both time-domain and frequency-domain Love numbers, for an extended set of linear viscoelastic constitutive equations that also include a transient response, like Burgers or Andrade rheologies. Generalized linear rheologies that until now have been utilized in flat geometry like the one characterizing the generalized Burgers material (Ivins et al. 2020) could be possibly implemented as well. Furthermore, `ALMA`^{3} can compute the time-derivatives of the Love numbers, and can deal with step-like and ramp-shaped forcing functions. The resulting Love numbers can be linearly superposed to obtain the planet response to arbitrarily time evolving loads. The versatility of `ALMA`^{3} has been demonstrated by a few examples, in which the Love numbers and some associated quantities like the quality factor Q, have been evaluated for some multi-layered models of planetary interiors characterized by complex rheological profiles.

ACKNOWLEDGMENTS

DM is funded by a INGV (Istituto Nazionale di Geofisica e Vulcanologia) 2020-23 "ricerca libera" research grant and by the INGV KINDLE grant. GS is funded by a FFABR (Finanziamento delle Attività Base di Ricerca) grant of MIUR (Ministero dell'Istruzione, dell'Università e della Ricerca) and by a research grant of DIFA (Dipartimento di Fisica e Astronomia "Augusto Righi") of the Alma Mater Studiorum Bologna University.

Data availability

Source code of the `ALMA`[3] version used to obtain numerical results presented in this work is available as a supplementary material. The data underlying plots shown in this article are available upon request to the corresponding author.

REFERENCES

Bamber, J. & Riva, R., 2010. The sea level fingerprint of recent ice mass fluxes, *The Cryosphere*, **4**(4), 621–627.

Bevis, M., Melini, D., & Spada, G., 2016. On computing the geoelastic response to a disk load, *Geophysical Journal International*, **205**(1), 1804–1812.

Buffett, B. A., 1997. Geodynamic estimates of the viscosity of the earth's inner core, *Nature*, **388**, 1476–4687.

Čadek, O., Tobie, G., Van Hoolst, T., Massé, M., Choblet, G., Lefèvre, A., Mitri, G., Baland, R.-M., Běhounková, M., Bourgeois, O., & Trinh, A., 2016. Enceladus's internal ocean and ice shell constrained from Cassini gravity, shape, and libration data, *Geophysical Research Letters*, **43**(11), 5653–5660.

Christensen, R., 1982. *Theory of Viscoelasticity*, Dover, Mineola, New York.

Clausen, N. & Tilgner, A., 2015. Dissipation in rocky planets for strong tidal forcing, *Astronomy & Astrophysics*, **584**, A60.

Cole, D. M. & Durell, G. D., 1995. The cyclic loading of saline ice, *Philosophical Magazine A*, **72**(1), 209–229.

Cottrell, A. H., 1996. Andrade creep, *Philosophical Magazine Letters*, **73**(1), 35–36.

Dumberry, M. & Mound, J., 2010. Inner core–mantle gravitational locking and the super-rotation of the inner core, *Geophysical Journal International*, **181**(2), 806–817.

Dumoulin, C., Tobie, G., Verhoeven, O., Rosenblatt, P., & Rambaux, N., 2017. Tidal constraints on the interior of Venus, *Journal of Geophysical Research: Planets*, **122**(6), 1338–1352.

Efroimsky, M. & Lainey, V., 2007. Physics of bodily tides in terrestrial planets and the appropriate scales of dynamical evolution, *Journal of Geophysical Research: Planets*, **112**, E12003.

Farrell, W., 1972. Deformation of the Earth by surface loads, *Reviews of Geophysics*, **10**(3), 761–797.

Farrell, W. & Clark, J., 1976. On postglacial sea level, *Geophysical Journal International*, **46**, 647–667.

Friederich, W. & Dalkolmo, J., 1995. Complete synthetic seismograms for a spherically symmetric earth by a numerical computation of the Green's function in the frequency domain, *Geophysical Journal International*, **122**(2), 537–550.

Garcia, R. F., Gagnepain-Beyneix, J., Chevrot, S., & Lognonné, P., 2011. Very preliminary reference Moon model, *Physics of the Earth and Planetary Interiors*, **188**(1), 96–113.

Garcia, R. F., Gagnepain-Beyneix, J., Chevrot, S., & Lognonné, P., 2012. Erratum to "Very Preliminary

Reference Moon Model", by R.F. Garcia, J. Gagnepain-Beyneix, S. Chevrot, P. Lognonné [Phys. Earth Planet. Inter. 188 (2011) 96–113], *Physics of the Earth and Planetary Interiors*, **202-203**, 89–91.

Gaver, D. P., 1966. Observing stochastic processes, and approximate transform inversion, *Operations Research*, **14**(3), 444–459.

Gavrilov, S. & Zharkov, V., 1977. Love numbers of the giant planets, *Icarus*, **32**(4), 443–449.

Goldreich, P. & Soter, S., 1966. Q in the solar system, *Icarus*, **5**(1), 375–389.

Harada, Y., Goossens, S., Matsumoto, K., Yan, J., Ping, J., Noda, H., & Haruyama, J., 2014. Strong tidal heating in an ultralow-viscosity zone at the core–mantle boundary of the Moon, *Nature Geoscience*, **7**, 569–572.

Harada, Y., Goossens, S., Matsumoto, K., Yan, J., Ping, J., Noda, H., & Haruyama, J., 2016. The deep lunar interior with a low-viscosity zone: Revised constraints from recent geodetic parameters on the tidal response of the Moon, *Icarus*, **276**, 96–101.

Heffels, A., Knapmeyer, M., Oberst, J., & Haase, I., 2021. Re-evaluation of Apollo 17 Lunar Seismic Profiling Experiment data including new LROC-derived coordinates for explosive packages 1 and 7, at Taurus-Littrow, Moon, *Planetary and Space Science*, **206**, 105307.

Hemingway, D., Iess, L., Tajeddine, R., & G., G. T., 2018. The interior of enceladus, in *Enceladus and the Icy Moons of Saturn*, pp. 57–77, eds Schenk, P. M., Clark, R. N., Howett, C. J. A., Verbiscer, A. J., & Waite, J. H., University of Arizona, Tucson.

Iess, L., Stevenson, D., Parisi, M., Hemingway, D., Jacobson, R., Lunine, J., Nimmo, F., Armstrong, J., Asmar, S., Ducci, M., et al., 2014. The gravity field and interior structure of Enceladus, *Science*, **344**(6179), 78–80.

Ivins, E. R., Caron, L., Adhikari, S., Larour, E., & Scheinert, M., 2020. A linear viscoelasticity for decadal to centennial time scale mantle deformation, *Reports on Progress in Physics*, **83**(10), 106801.

Kaula, W. M., 1964. Tidal dissipation by solid friction and the resulting orbital evolution, *Reviews of Geophysics*, **2**(4), 661–685.

Kellermann, C., Becker, A., & Redmer, R., 2018. Interior structure models and fluid Love numbers of exoplanets in the super-Earth regime, *Astronomy & Astrophysics*, **615**, A39.

Koot, L. & Dumberry, M., 2011. Viscosity of the Earth's inner core: Constraints from nutation observations, *Earth and Planetary Science Letters*, **308**(3), 343–349.

Lambeck, K., 1988. The earth's variable rotation: some geophysical causes, in *Symposium-International Astronomical Union*, vol. 128, pp. 1–20, Cambridge University Press.

Love, A. E. H., 1911. *Some Problems of Geodynamics: Being an Essay to which the Adams Prize in the University of Cambridge was Adjudged in 1911*, CUP Archive.

Melini, D., Cannelli, V., Piersanti, A., & Spada, G., 2008. Post-seismic rebound of a spherical Earth: new insights from the application of the Post-Widder inversion formula, *Geophysical Journal International*, **174**(2), 672–695.

Melini, D., Gegout, P., King, M., Marzeion, B., & Spada, G., 2015a. On the rebound: Modeling Earth's ever-changing shape, *Eos T. Am. Geophys. Un.*, **96**.

Michel, A. & Boy, J.-P., 2021. Viscoelastic Love numbers and long period geophysical effects, *Geophysical Journal International*, ggab369.

Mitrovica, J. X., 1996. Haskell [1935] revisited, *Journal of Geophysical Research: Solid Earth*, **101**(B1), 555–569.

Munk, W. H. & MacDonald, G. J., 1960. *The Rotation of the Earth: A Geophysical Discussion*, Cambridge Univ. Press, New York.

Murray, C. D. & Dermott, S. F., 2000. *Solar System Dynamics*, Cambridge University Press.

Nield, G., Barletta, V., Bordoni, A., King, M., Whitehouse, P., Clarke, P., Domack, E., Scambos, T., & Berthier, E., 2014. Rapid bedrock uplift in the Antarctic Peninsula explained by viscoelastic response to recent ice unloading, *Earth and Planetary Science Letters*, **397**, 32–41.

Nunn, C., Garcia, R. F., Nakamura, Y., Marusiak, A. G., Kawamura, T., Sun, D., Margerin, L., Weber, R., Drilleau, M., Wieczorek, M. A., Khan, A., Rivoldini, A., Lognonné, P., & Zhu, P., 2020. Lunar seismology: A data and instrumentation review, *Space Science Reviews*, **216**(89).

Organowski, O. & Dumberry, M., 2020. Viscoelastic relaxation within the Moon and the phase lead of its Cassini state, *Journal of Geophysical Research: Planets*, **125**(7), e2020JE006386.

Padovan, S., Spohn, T., Baumeister, P., Tosi, N., Breuer, D., Csizmadia, S., Hellard, H., & Sohl, F., 2018. Matrix-propagator approach to compute fluid Love numbers and applicability to extrasolar planets, *Astronomy & Astrophysics*, **620**, A178.

Peltier, W. & Drummond, R., 2008. Rheological stratification of the lithosphere: A direct inference based upon the geodetically observed pattern of the glacial isostatic adjustment of the North American continent, *Geophysical Research Letters*, **35**(16).

Peltier, W. R., 1974. The impulse response of a Maxwell Earth, *Review of Geophysics and Space Physics*, **12**(4), 649–669.

Pollitz, F. F., 2003. Transient rheology of the uppermost mantle beneath the Mojave Desert, California, *Earth and Planetary Science Letters*, **215**(1-2), 89–104.

Pollitz, F. F., 2005. Transient rheology of the upper mantle beneath central Alaska inferred from the crustal velocity field following the 2002 Denali earthquake, *Journal of Geophysical Research: Solid Earth*, **110**(B8).

Porco, C. C., Helfenstein, P., Thomas, P., Ingersoll, A., Wisdom, J., West, R., Neukum, G., Denk, T., Wagner, R., Roatsch, T., et al., 2006. Cassini observes the active south pole of Enceladus, *Science*, **311**(5766), 1393–1401.

Post, E. L., 1930. Generalized differentiation, *Transactions of the American Mathematical Society*, **32**(4), 723–781.

Purcell, A., Tregoning, P., & Dehecq, A., 2016. An assessment of the ICE6G_C (VM5a) glacial isostatic adjustment model, *Journal of Geophysical Research: Solid Earth*, **121**(5), 3939–3950.

Qiu, Q., Moore, J. D. P., Barbot, S., Feng, L., & Hill, E. M., 2018. Transient rheology of the Sumatran mantle wedge revealed by a decade of great earthquakes, *Nature Communications*, **9**(1), 995.

Rambaux, N., Castillo-Rogez, J. C., Williams, J. G., & Karatekin, Ö., 2010. Librational response of Enceladus, *Geophysical Research Letters*, **37**(4).

Riva, R. E. M. & Vermeersen, L. L. A., 2002. Approximation method for high-degree harmonics in normal mode modelling, *Geophysical Journal International*, **151**(1), 309–313.

Roberts, J. H., 2015. The fluffy core of Enceladus, *Icarus*, **258**, 54–66.

Roberts, J. H. & Nimmo, F., 2008. Tidal heating and the long-term stability of a subsurface ocean on enceladus, *Icarus*, **194**(2), 675–689.

Rundle, J. B., 1982. Viscoelastic-gravitational deformation by a rectangular thrust fault in a layered Earth, *Journal of Geophysical Research: Solid Earth*, **87**(B9), 7787–7796.

Sabadini, R., Yuen, D. A., & Boschi, E., 1982. Polar wandering and the forced responses of a rotating, multilayered, viscoelastic planet, *Journal of Geophysical Research: Solid Earth*, **87**(B4), 2885–2903.

Saito, M., 1978. Relationship between tidal and load Love numbers, *Journal of Physics of the Earth*, **26**(1), 13–16.

Shida, T., 1912. *On the elasticity of the Earth and the Earth's crust*, Kyoto Imperial University.

Silverii, F., D'Agostino, N., Métois, M., Fiorillo, F., & Ventafridda, G., 2016. Transient deformation of karst aquifers due to seasonal and multiyear groundwater variations observed by GPS in southern Apennines (Italy), *Journal of Geophysical Research: Solid Earth*, **121**(11), 8315–8337.

Slangen, A., 2012. *Modelling regional sea–level changes in recent past and future*, Ph.D. thesis, Utrecht University, the Netherlands.

Smith, D., 2003. Using multiple-precision arithmetic, *Computing in Science Engineering*, **5**(4), 88–93.

Smith, D. M., 1991. Algorithm 693: A FORTRAN Package for Floating-Point Multiple-Precision Arithmetic,

ACM Trans. Math. Softw., **17**(2), 273–283.

Sohl, F., Hussmann, H., Schwentker, B., Spohn, T., & Lorenz, R. D., 2003. Interior structure models and tidal Love numbers of Titan, *Journal of Geophysical Research: Planets*, **108**(E12).

Spada, G., 2008. ALMA, a Fortran program for computing the viscoelastic Love numbers of a spherically symmetric planet, *Computers & Geosciences*, **34**(6), 667–687.

Spada, G. & Boschi, L., 2006. Using the Post-Widder formula to compute the Earth's viscoelastic Love numbers, *Geophysical Journal International*, **166**(1), 309–321.

Spada, G. & Melini, D., 2019. SELEN^4 (SELEN version 4.0): a Fortran program for solving the gravitationally and topographically self-consistent sea-level equation in glacial isostatic adjustment modeling, *Geoscientific Model Development*, **12**(12), 5055–5075.

Spada, G., Barletta, V. R., Klemann, V., Riva, R., Martinec, Z., Gasperini, P., Lund, B., Wolf, D., Vermeersen, L., & King, M., 2011. A benchmark study for glacial isostatic adjustment codes, *Geophysical Journal International*, **185**(1), 106–132.

Stehfest, H., 1970. Algorithm 368: Numerical inversion of Laplace transforms [D5], *Communications of the ACM*, **13**(1), 47–49.

Sun, W. & Okubo, S., 1993. Surface potential and gravity changes due to internal dislocations in a spherical earth—I. Theory for a point dislocation, *Geophysical Journal International*, **114**(3), 569–592.

Tanaka, Y., Okuno, J., & Okubo, S., 2006. A new method for the computation of global viscoelastic post-seismic deformation in a realistic earth model (I)—vertical displacement and gravity variation, *Geophysical Journal International*, **164**(2), 273–289.

Thomson, W., 1863. XXVII. On the rigidity of the earth, *Philosophical Transactions of the Royal Society of London*, **153**, 573–582.

Tobie, G., Grasset, O., Dumoulin, C., & Mocquet, A., 2019. Tidal response of rocky and ice-rich exoplanets, *Astronomy & Astrophysics*, **630**, A70.

Turcotte, D. L. & Schubert, G., 2014. *Geodynamics - Applications of Continuum Physics to Geological Problems*, Cambridge University Press.

Valkó, P. P. & Abate, J., 2004. Comparison of sequence accelerators for the Gaver method of numerical Laplace transform inversion, *Computers & Mathematics with Applications*, **48**(3), 629–636.

Vaughan, D. G., 1995. Tidal flexure at ice shelf margins, *Journal of Geophysical Research: Solid Earth*, **100**(B4), 6213–6224.

Vermeersen, L. & Mitrovica, J., 2000. Gravitational stability of spherical self-gravitating relaxation models, *Geophysical Journal International*, **142**(2), 351–360.

Wahr, J., Selvans, Z. A., Mullen, M. E., Barr, A. C., Collins, G. C., Selvans, M. M., & Pappalardo, R. T., 2009. Modeling stresses on satellites due to nonsynchronous rotation and orbital eccentricity using gravitational potential theory, *Icarus*, **200**(1), 188–206.

Weber, R. C., Lin, P.-Y., Garnero, E. J., Williams, Q., & Lognonné, P., 2011. Seismic detection of the lunar core, *Science*, **331**(6015), 309–312.

Widder, D. V., 1934. The inversion of the Laplace integral and the related moment problem, *Transactions of the American Mathematical Society*, **36**(1), 107–200.

Williams, J. G. & Boggs, D. H., 2015. Tides on the Moon: Theory and determination of dissipation, *Journal of Geophysical Research: Planets*, **120**(4), 689–724.

Williams, J. G., Konopliv, A. S., Boggs, D. H., Park, R. S., Yuan, D.-N., Lemoine, F. G., Goossens, S., Mazarico, E., Nimmo, F., Weber, R. C., Asmar, S. W., Melosh, H. J., Neumann, G. A., Phillips, R. J., Smith, D. E., Solomon, S. C., Watkins, M. M., Wieczorek, M. A., Andrews-Hanna, J. C., Head, J. W., Kiefer, W. S., Matsuyama, I., McGovern, P. J., Taylor, G. J., & Zuber, M. T., 2014. Lunar interior properties from the GRAIL mission, *Journal of Geophysical Research: Planets*, **119**(7), 1546–1578.

Wu, P. & Ni, Z., 1996. Some analytical solutions for the viscoelastic gravitational relaxation of a two-layer

non-self-gravitating incompressible spherical earth, *Geophysical Journal International*, **126**(2), 413–436.

Wu, P. & Peltier, W., 1982. Viscous gravitational relaxation, *Geophysical Journal International*, **70**(2), 435–485.

Zhang, C., 1992. Love numbers of the Moon and of the terrestrial planets, *Earth, Moon, and Planets*, **56**(3), 193–207.

Rheological law	Complex rigidity $\mu(s)$
Hooke	μ
Maxwell	$\dfrac{\mu s}{s+\mu/\eta}$
Newton	$\eta\, s$
Kelvin	$\mu+\eta s$
Burgers	$\dfrac{\mu s\left(s+\dfrac{\mu_2}{\eta_2}\right)}{s^2+s\left(\dfrac{\mu}{\eta}+\dfrac{\mu+\mu_2}{\eta_2}\right)+\dfrac{\mu\,\mu_2}{\eta\,\eta_2}}$
Andrade	$\left[\dfrac{1}{\mu}+\dfrac{1}{\eta s}+\Gamma(\alpha+1)\dfrac{1}{\mu}\left(\dfrac{\eta s}{\mu}\right)^{-\alpha}\right]^{-1}$

Table 1. Complex rigidities $\mu(s)$ for the linear viscoelastic rheologies implemented in `ALMA`[3]. Here, μ is the elastic rigidity, η is the newtonian viscosity, μ_2 and η_2 are the rigidity and viscosity of the transient element in the bi-viscous Burgers rheology, respectively. In the Andrade rheological law, α is the creep parameter while $\Gamma(x)$ denotes the Gamma function.

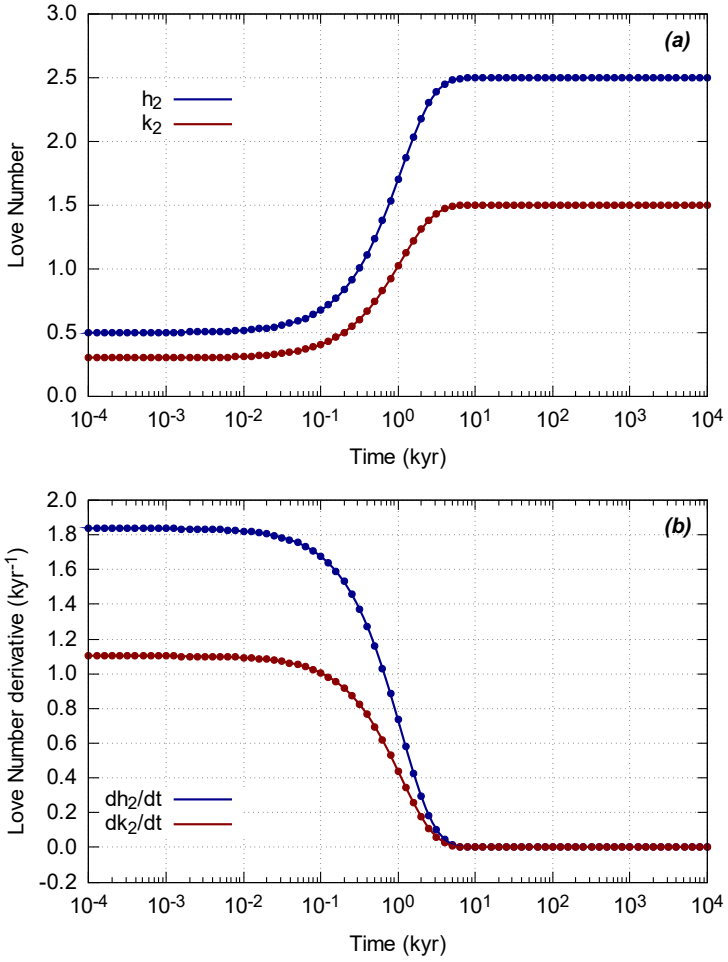

Figure 1. (a) Benchmark comparison between numerical (dotted) and analytical solutions (solid) for the tidal LNs h and k of degree $n = 2$, for a Kelvin sphere with Maxwell rheology having radius $a = 6371$ km, density $\rho = 5.514 \times 10^3$ kg·m^{-3}, rigidity $\mu = 1.46 \times 10^{11}$ Pa and viscosity $\eta = 10^{21}$ Pa·s. The model has been set up with a central core of radius $c = 3480$ km and a mantle, both having the same rheological parameters. (b) The same, for the time derivatives of the LNs. In both cases, `ALMA`^{3} has been configured with parameters $M = 8$ and $D = 128$. Note that the time axis is logarithmic.

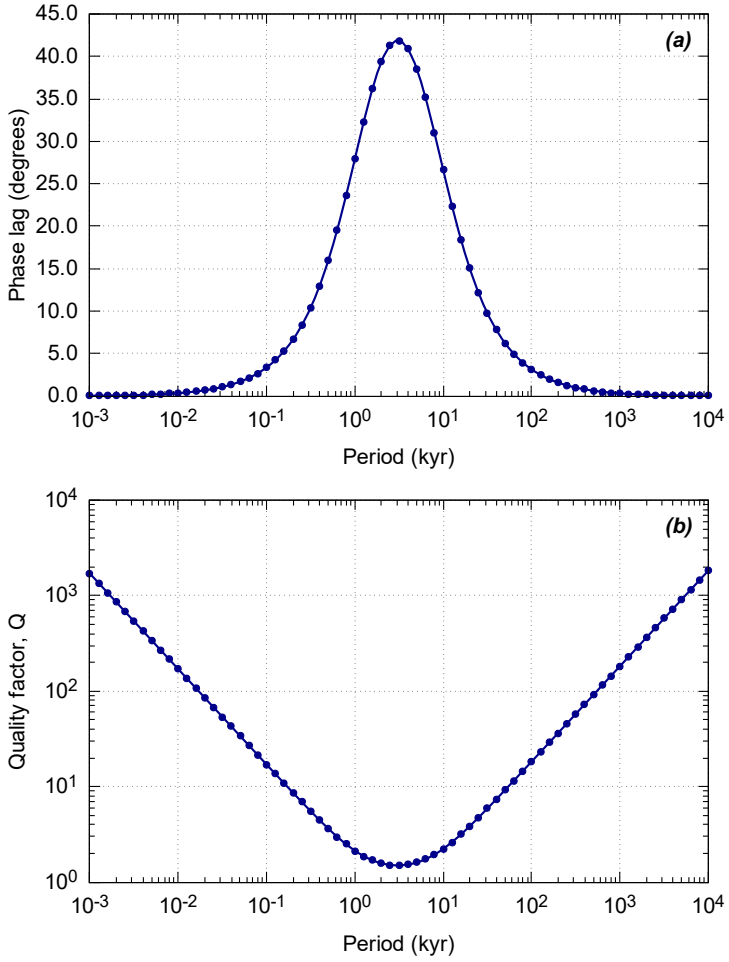

Figure 2. Benchmark comparison between numerical (dotted) and analytical solutions (solid) for the tidal phase lag ϕ (a) and quality factor Q (b) for the Kelvin sphere with Maxwell rheology, using the same parameters detailed in the caption of Figure 1.

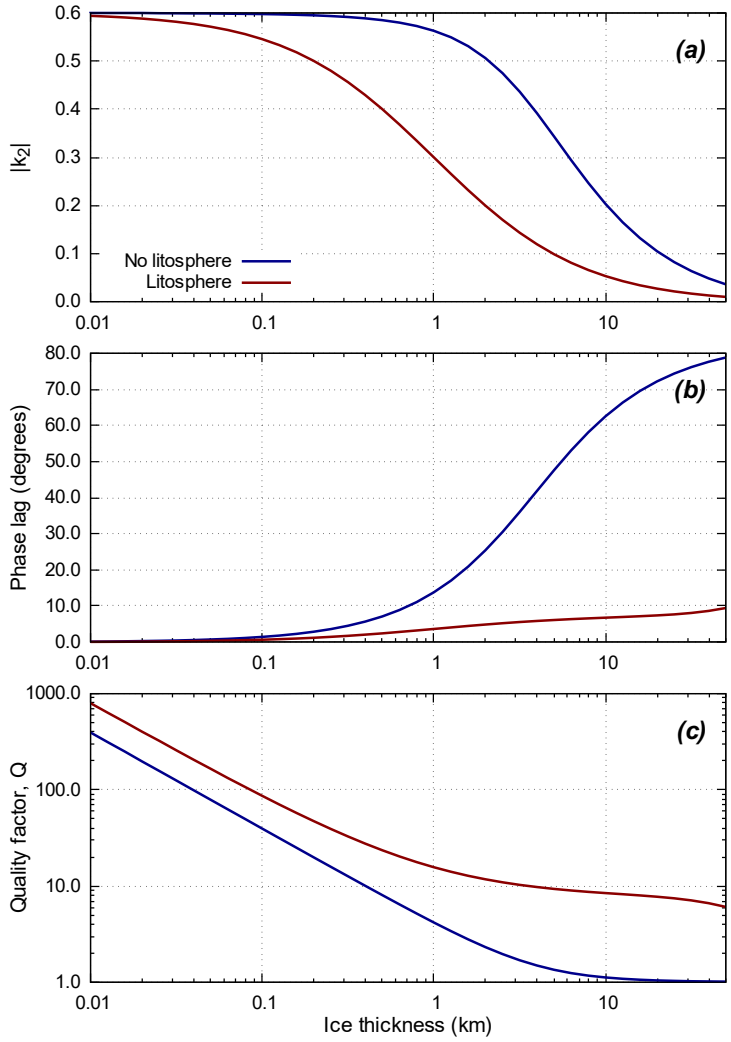

Figure 3. Modulus of tidal Love number $|k_2|$ for Enceladus (frame a), phase lag (b) and quality factor (c) as a function of the thickness of the ice shell, for a forcing period $T = 1.37$ days. Blue curves correspond to a uniform ice shell with viscosity $\eta_i = 10^{13}$ Pa·s, while for red curves an high-viscosity ($\eta_l = 10^{19}$ Pa·s) ice litosphere is assumed in the upper half of the shell.

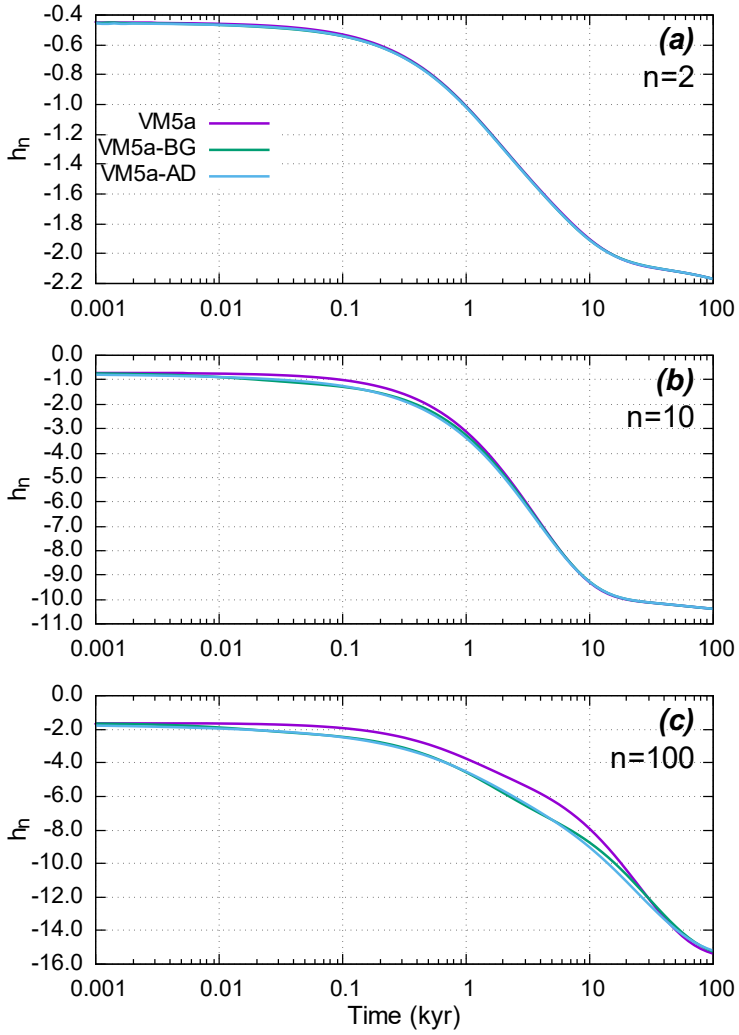

Figure 4. Loading Love number $h_n(t)$ for $n = 2$ (frame a), $n = 10$ (b) and $n = 100$ (c), obtained with the VM5a viscosity model by Peltier & Drummond (2008) and with two variants that assume Burgers (VM5a-BG) or Andrade (VM5a-AD) rheologies in the upper mantle layers.

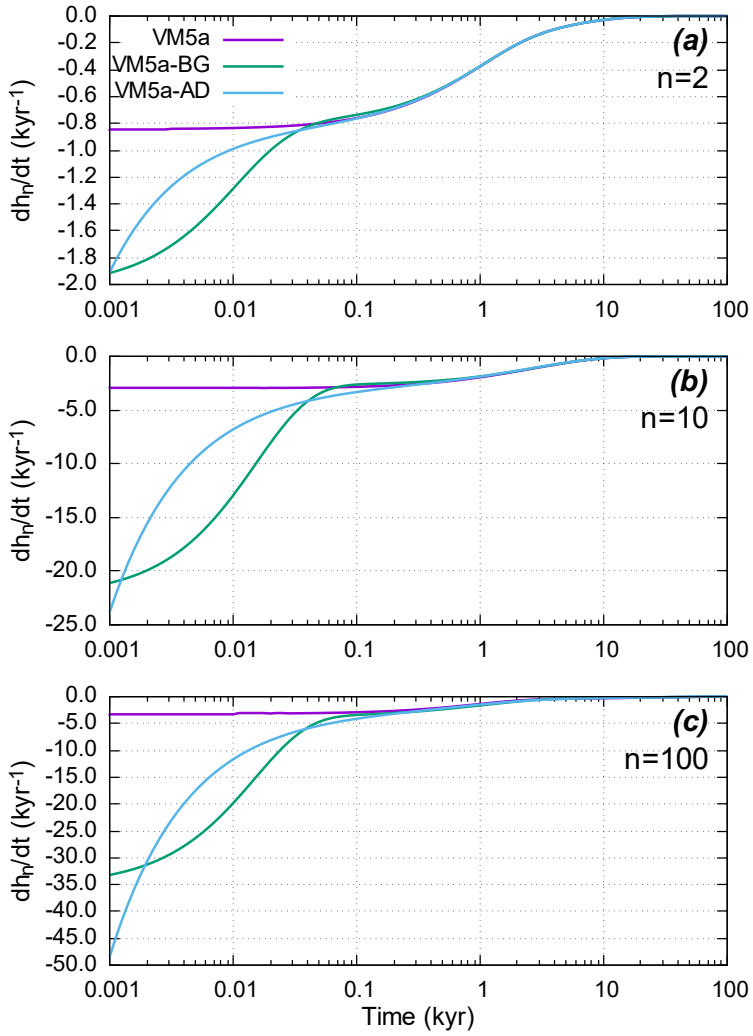

Figure 5. Time-derivative of the loading Love number $\dot{h}_n(t)$ for $n = 2, 10$ and 100, for the rheological models described in the caption of Figure 4.

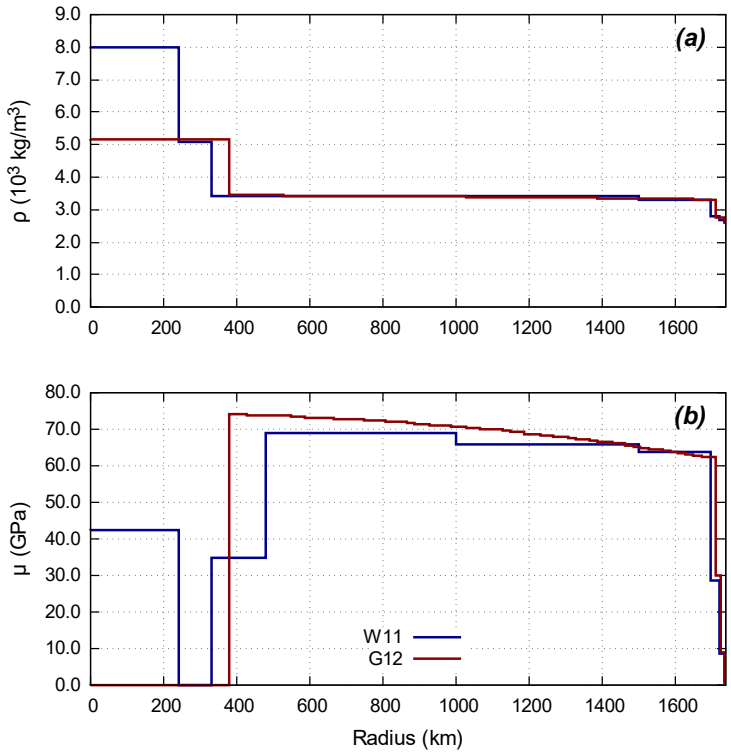

Figure 6. Radial profiles of density (a) and rigidity (b) for the Moon models by Weber et al. (2011) (W11, blue) and Garcia et al. (2011, 2012) (G12, red).

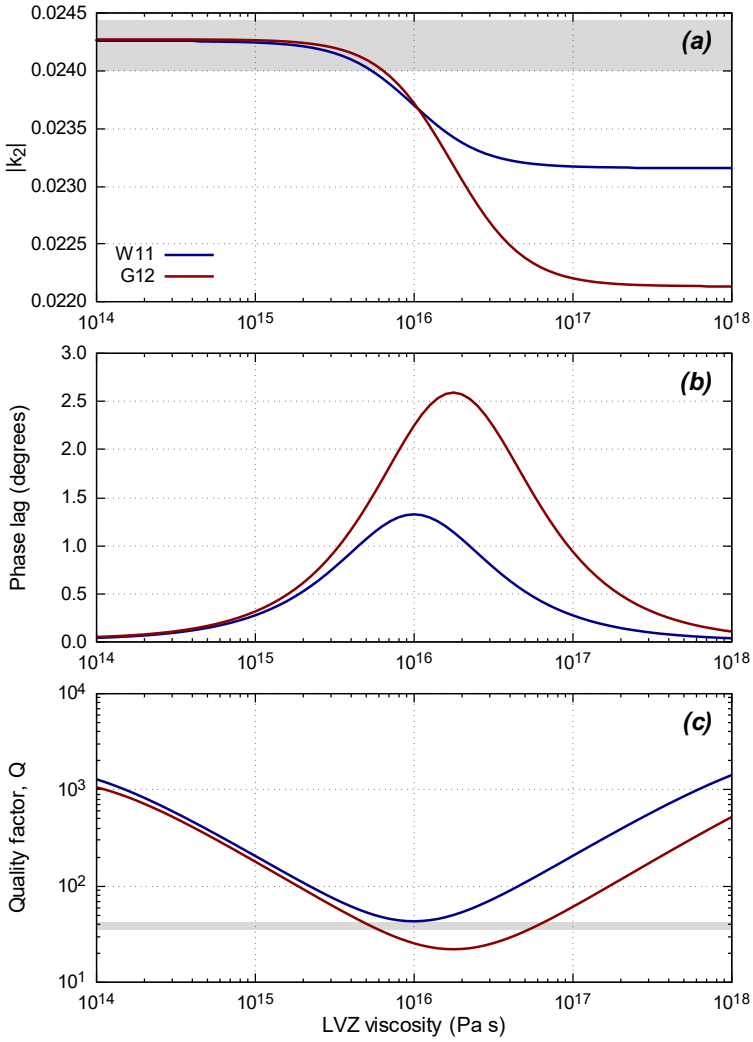

Figure 7. Modulus of the tidal Love number $|k_2|$ for the Moon (frame a), phase lag (b) and quality factor (c) as a function of the LVZ viscosity, for a forcing period $T = 27.212$ days. Blue and red curves correspond to the Moon models by Weber et al. (2011) and Garcia et al. (2011, 2012) shown in Figure 6. Shaded areas in frames (a) and (c) correspond to the 1-σ confidence intervals for measured values of k_2 and Q (Williams & Boggs 2015).